Aerodynamic Interaction Between Propellers and Wings

Dave P. Witkowski,* Alex K. H. Lee,* and John P. Sullivan†
Purdue University, West Lafayette, Indiana

A combined experimental and computational investigation of the aerodynamic interaction between propellers and wings has been conducted at the Purdue University Aerospace Sciences Laboratory. This study's primary objective was the determination of the time-averaged performance of a propeller and wing in a tractor configuration. A wind-tunnel test was performed using an untapered, semispan wing and a Purdue model propeller mounted in a tractor arrangement. All tests were conducted at low subsonic speeds, $M = 0.1$, and a Reynolds number of 470,000 based on the wing chord of 8 in. A computational analysis utilizing two individual methods was performed. A semiempirical model that calculated wing performance for a predetermined steady propeller-wake velocity distribution was formulated. The second method was a vortex lattice simulation of both the propeller and wing, which is capable of calculating the quasisteady loadings. The results of the experiment and the computational analysis showed good agreement and indicated a significant steady-state performance improvement for the tractor configuration, including a reduction in wing-induced drag and increases in propeller efficiency and wing lift curve slope. The quasisteady results of the computational analysis provided insight into the time-dependent loadings on both the propeller and wing.

Nomenclature

A_{ij} = influence coefficient matrix
b = full wingspan, 66 in.
C_D = wing drag coefficient, drag/qS
C_L = wing lift coefficient, lift/qS
C_{L_α} = wing lift curve slope, 1/rad
C_P = propeller power coefficient, $2\pi n\tau/\rho n^3 D^5$
C_T = propeller thrust coefficient, $T/\rho n^2 D^4$
c = wing chord, 8 in.
c_d = section drag coefficient, D_i/qc
c_l = section lift coefficient, L/qc
D = propeller diameter
D_i = section-induced drag
F = section force, $\rho V_R \Gamma$
J = propeller advance ratio, U_∞/nD
L = section lift
M = Mach number
n = propeller rotational speed, rev/s
q = dynamic pressure
R = propeller radius
r = radial distance from propeller axis
S = exposed wing planform area, 264 in.^{2}
T = propeller thrust
U_∞ = freestream velocity
u_p = propeller-induced axial velocity
V_R = resultant velocity
w_p = propeller-induced vertical velocity
w_w = wing-induced vertical velocity
y_p = spanwise propeller location, from wing root
Z.L.L. = section zero lift line
α = geometric angle of attack
α_{eff} = effective angle of attack
α_i = induced angle of attack
Γ_i^N = circulation of element i of blade N or wing W
η = propeller propulsive efficiency, JC_T/C_p
η_{eff} = effective efficiency
ω = propeller rotational speed, rad/s
ρ = air density
τ = propeller torque

Presented as Paper 88-0665 at the AIAA 26th Aerospace Sciences Meeting, Reno, NV, Jan. 11-14, 1988; received Feb. 16, 1988; revision received Feb. 28, 1989.

*Research Assistant. Student Member AIAA.
†Professor, Aeronautics and Astronautics. Member AIAA.

Introduction

IN an effort to alleviate the problem of rising fuel cost, aircraft designers are again considering propellers as a viable propulsion alternative for the future. As a result, recent efforts have been directed toward an attempt to make propellers even more fuel efficient over wider operating conditions. Examples of such innovations on the propeller propulsive system include advanced blade airfoil sections, blade sweep, spinner area ruling, and counter-rotation. However, inherent to the consideration of propellers as an aircraft propulsion system is the problem of interaction between the propeller and other aerodynamic surfaces of the aircraft. This interaction can affect aircraft stability and aerodynamic performance, as well as generate noise and vibration. As a result, engineers must investigate methods of integrating the propeller and aircraft for optimum installed efficiency in addition to improving the performance of isolated propeller systems.

For wing-mounted configurations, the integration aspect that will have the greatest impact on the overall aerodynamic performance of the aircraft is the interaction between the propeller and the wing. Propeller/wing interaction has recently been studied both experimentally and analytically. Computational codes that predict the optimum wing lift distribution for tractor and pusher configurations have been developed by Kroo[1] and Miranda and Brennan.[2] Both methods showed that significant wing drag reduction can be accomplished for an optimized tractor configuration, and significant propeller efficiency improvement can be obtained for the pusher configuration. Wind-tunnel tests performed by Patterson and Bartlett[3] confirmed the latter of these results.

This investigation comprises a complementary experimental and computational effort that addresses the effect of interaction on the steady performance of a propeller and wing in a tractor configuration. In order to determine the magnitude

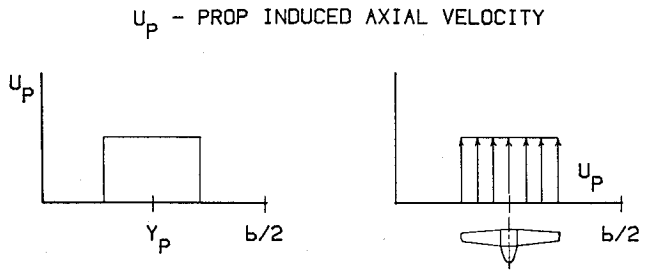

Fig. 1a Distribution of induced axial velocities in the model propeller wake.

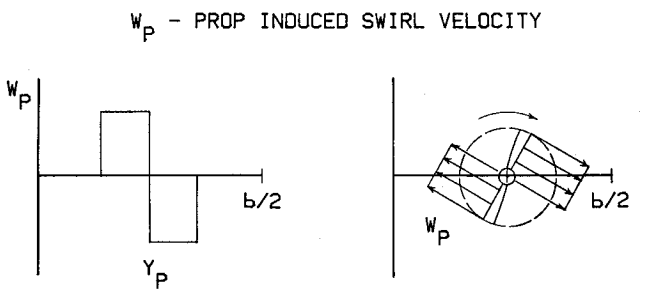

Fig. 1b Distribution of induced tangential velocities in the model propeller wake.

and characteristics of the anticipated performance benefits, a wind-tunnel test was performed in the Purdue University Low-Speed Subsonic Wind Tunnel on a tractor configuration with a rectangular semispan wing and a Purdue model propeller.

The computational analysis was conducted using two different methods. A semiempirical method for a tractor configuration was formulated as an experimental design tool for predicting interaction effects on a wing of specified geometry. This method involved the superposition of experimentally correlated propeller wake velocities onto the uniform freestream flow ahead of a wing modeled by the vortex lattice method. In addition to the design code, a vortex lattice simulation of both the wing and propeller was developed. By simultaneously solving for the circulation distributions of the propeller and wing, the performance of both of these components was determined under the mutually interactive conditions of normal operation. An additional feature of this vortex lattice model is that the simultaneous solution of the propeller and wing enables the quasisteady loadings to be calculated. These quasisteady results can be related to time-dependent aerodynamic forcing functions, which induce structural vibration and noise. The steady results of both models were compared to the experimental data.

Design Philosophy

It has long been known that a substantial portion of the power consumed by a propeller system is wasted on the generation of a tangential or swirl velocity, which in no way contributes to the thrust. Techniques such as counter-rotation and stationary guide vanes or stators have been employed successfully as methods of improving propeller efficiency by recovering the swirl kinetic energy. These techniques operate on the principle that an aerodynamic surface can be introduced into the wake of a swirl-producing body in order to divert the swirl component of velocity into the streamwise direction, therefore augmenting the thrust or diminishing the drag of the combination. By the same logic, it should be feasible to achieve some performance benefit from a propeller and wing combination.

In an effort to simultaneously gain a physical understanding of this problem and estimate the performance changes for an effective experimental design, a simple semiempirical code was formulated.

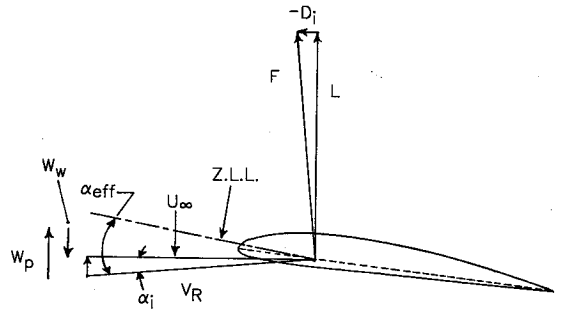

Fig. 2a Wing section in propeller upwash when $w_p > w_w$.

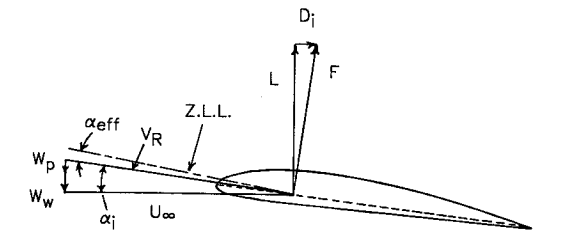

Fig. 2b Wing section in propeller downwash when $\alpha_{eff} > 0$.

Description of Semiempirical Design Code

The two major assumptions of this model are that propeller performance is not altered by the presence of the wing and that propeller wake velocities are steady. Thus, from the first assumption, the model is good only for the tractor configuration. The propeller wake velocities are superimposed onto a wing modeled by the vortex lattice method. The code input consists of steady velocity distributions in the propeller wake and wing geometry. The results consist of the total and sectional wing lift and drag. Propeller velocity distributions were chosen as constant over the wake area (see Fig. 1), which is a good representation of the Purdue model propeller wake at moderate to high advance ratios as shown by the laser velocimeter measurements of Sundar.[4] The propeller wake velocity magnitudes were correlated to isolated propeller performance data by a modified momentum analysis.[5] Viscous drag on the wing was simulated by a strip analysis coupled with two-dimensional airfoil drag data.[6]

Wing Performance

Although the primary benefit experienced in a pusher configuration is a propeller thrust increase,[1-3] the performance improvement associated with a tractor configuration manifests itself mainly as a wing-induced drag reduction. This effect results from the modification of the local angles of attack on the wing by the tangential velocity in the propeller wake. Essentially, the propeller induces an "effective twist" on the portion of the wing, which is immersed in the propeller wake.

The generation of an induced drag on isolated finite wings is well known. The vortical flow in the wake of a lifting finite wing induces a downwash, which acts to decrease the local incident flow angle and rotate the resultant force vector back. This vector rotation creates an induced-drag component on the wing.

In the tractor arrangement, the propeller swirl produces regions of upwash and downwash on the wing. Figure 1b illustrates this effect for the inboard up rotation case. In the upwash region, the propeller swirl counteracts the effects of the wing downwash such that the local angles of attack are increased. This effect simultaneously augments the section lift and rotates the force vector forward, which reduces the drag component at the section. Figure 2a illustrates the wing-section loading in the upwash region for the case where propeller swirl is greater than the wing downwash. Under these conditions, the rotation angle is great enough to tilt the force vector forward, creating a localized wing thrust at the section.

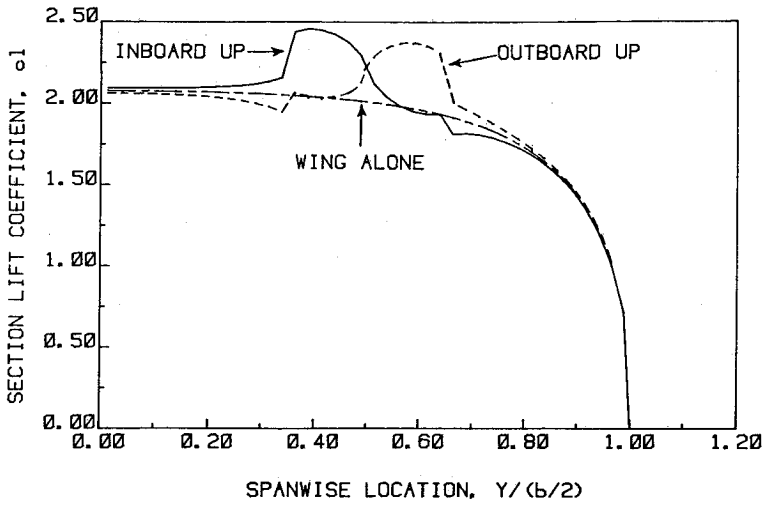

Fig. 2c Lift distribution results of the design calculation.

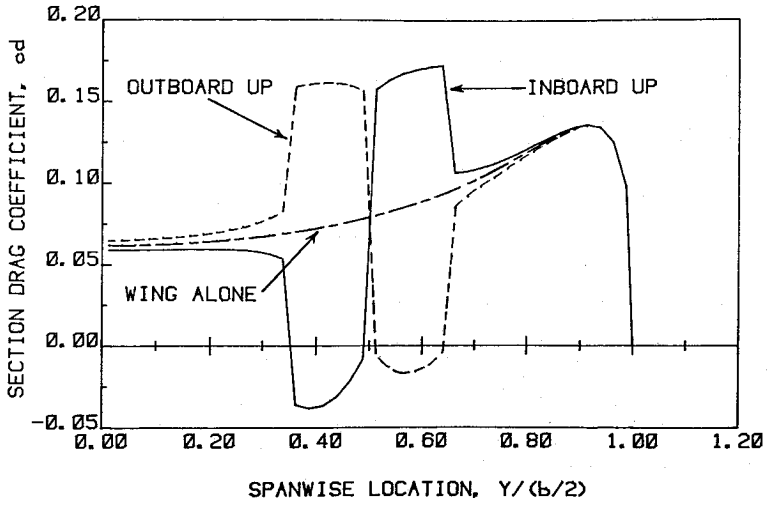

Fig. 2d Drag distribution results of the design calculation.

The propeller swirl and the wing downwash act together to further decrease the local angles of attack in the propeller downwash region. This simultaneously diminishes the section lift and pivots the force vector further back resulting in an increased section drag (Fig. 2b).

The results described above are evident in the lift and drag distributions obtained from the semiempirical design code in Figs. 2c and 2d, respectively. For most operating conditions, the opposing drag decrease in the upwash region and the drag increase in the downwash region of the propeller wake will not cancel. The main reason for this is that the rotated force vectors in the two region are not of the same magnitude. Thus, the necessary conditions for the wing drag reduction would require the backward rotated force in the propeller downwash region to be smaller than the forward rotated force in the propeller upwash region. Previous discussions reveal a natural tendency toward this condition since the force is augmented in the upwash region due to the local angle-of-attack increase and diminished in the downwash region due to the local angle-of-attack decrease. However, an additional factor to consider is the natural attenuation of the lift loading toward the wingtips of a finite wing. Taking this into account, it is readily apparent that locating the upwash region inboard of the downwash region is advantageous.

An additional effect of the propeller-wing interaction is an augmented wing lift, mostly due to the increase in axial velocity across the propeller wake.

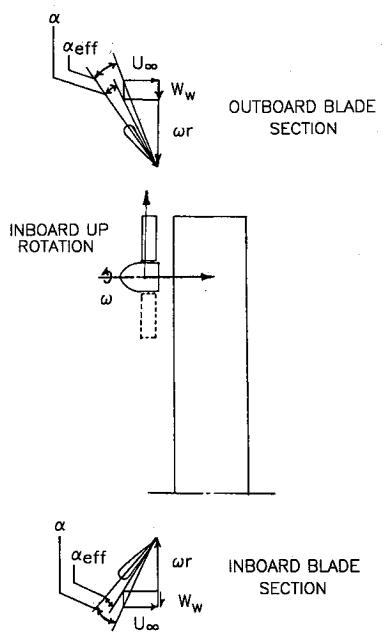

Fig. 3 Wing influence on the propeller

Propeller Performance

In addition to the wing effects, the upwash induced upstream of the wing alters the propeller performance by modifying the local angles of attack on the blades. Figure 3 shows that the downward rotating blade has a local angle-of-attack increase that increases the section lift, resulting in an augmented thrust and torque on the blade. The upward rotating blade experiences a local angle-of-attack decrease that diminishes the section lift, resulting in a decreased thrust and torque on the

blade. Since propeller geometry is more complex than wing geometry, it is more difficult to make a positive conclusion about whether propeller performance is expected to improve or degrade. However, these effects will vary sinusoidally over the propeller revolution and on averaging are expected to be smaller than the wing drag reduction. This occurs since only a component of the upwash acts to affect the blades in the manner described except when the blades are near the plane of the wing.

Geometric Considerations

The previous discussion provides insight into some of the features of this interference effect. One of the most elementary design choices with major consequences for interaction is direction of propeller rotation. Rotating the propeller such that the upwash region is inboard can be seen to be beneficial as discussed in the Wing Performance section. Results from the design code have indeed shown that wing drag actually increases for all but high propeller loadings when outboard up rotation is used.

Similarly, it is evident that drag is reduced further as the spanwise propeller location is moved outboard for moderate power loading and inboard up rotation. This results from the fact that the spanwise lift gradient is large toward the wingtips, which again indicates that the forward rotated vector is greater in magnitude than the backward rotated one. This point can be further illustrated if the propeller is located on the wingtip. In this case, the upwash acts as previously described, but the downwash does not act on the wing surface at all.

However, when the propeller is heavily loaded (large swirl velocities) and the wing geometric angle of attack is small, a negative local flow angle can be induced on the wing in the downwash region of the propeller wake. The resulting negative lift in the downwash region is tilted forward creating a local induced-thrust component on the wing in addition to the beneficial effects, which occur in the upwash region. The consequence of this effect is that inboard propeller locations are preferred under these conditions since larger forces are rotated forward across the entire propeller wake region.

It has been shown that it is reasonable to expect a time-averaged performance improvement for both the propeller and wing of a tractor configuration as a result of aerodynamic interaction. This improvement is anticipated upon the condition that certain design criteria are followed. However, experimental study is required if the nature and magnitude of these benefits are to be determined.

Experimental Setup and Procedure

Test Facility

The experimental portion of this investigation was performed at the Purdue University Aerospace Sciences Laboratory in the 3×4.5-ft Low-Speed Subsonic Wind Tunnel. The tests were conducted in the tunnel's closed test section where velocities of approximately 350 ft/s can be attained. Test-section dynamic pressure was maintained at a preset value by an electronic feedback system. A pitot-static probe upstream of the test configuration measured the dynamic pressure. Total temperature was measured by a thermocouple in the tunnel stilling section. Since all tests were conducted under nearly incompressible conditions, $M = 0.1$, static temperature was assumed to be equivalent to total temperature. Test-section static pressure was obtained by an electronic transducer referenced to ambient conditions.

Test Rig Configuration

A drawing of the tractor test rig that was used in the experiment is shown in Fig. 4. This setup was designed to independently measure steady propeller and wing loads while minimizing the amount of undesirable interference from struts, shafts, and nacelles. The small scale of the model necessitated the independent mounting of the propeller and wing. A pusher-type power train was selected, since it allowed the shaft axis to be vertically aligned with the quarter chord of the wing. In this alignment, the mutual interference effects are maximized. In order to assure beneficial interactive effects, propeller rotation was chosen to be inboard up. The streamwise distance between the quarter-chord lines of the propeller and the wing was 6 in. ($D/2$).

The unswept, untapered wing was floor mounted in a half-span configuration. This wing had a NACA 0012 airfoil section, a chord of 8 in., and an aspect ratio of 8.25 based on a full span of 66 in. The lift and drag on the wing were measured by a six-component, pyramidal, electric strain-gauge balance located under the tunnel floor. Since the wing was supported

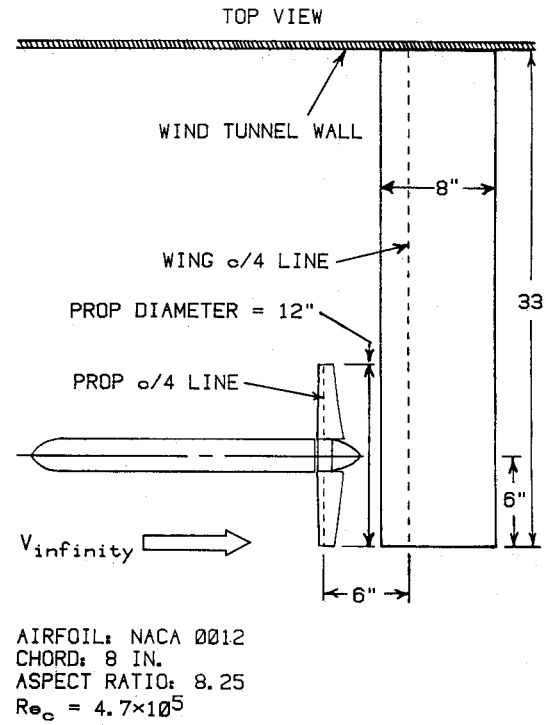

Fig. 4a Top view of the experimental test rig.

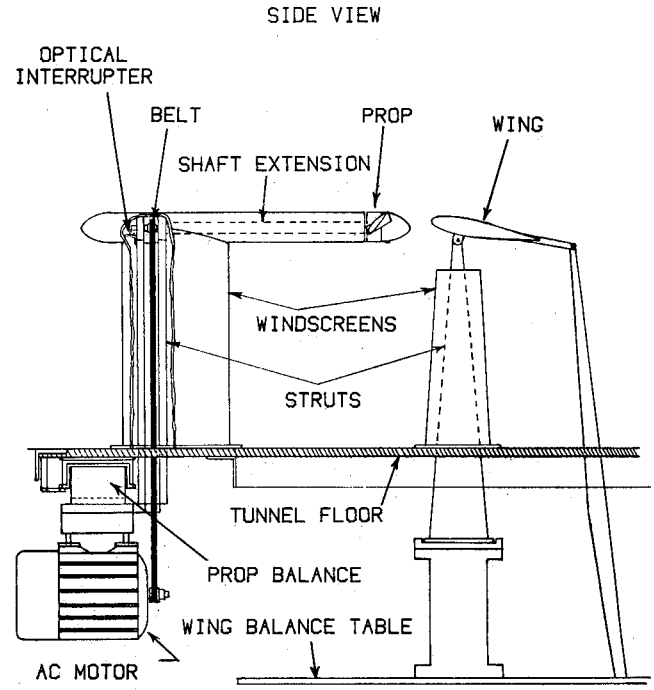

Fig. 4b Side view of the experimental test rig.

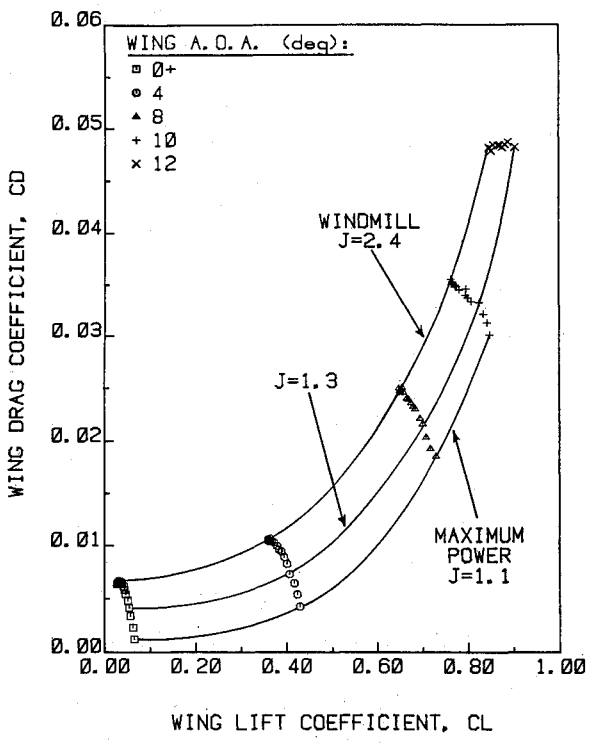

Fig. 5 Wing drag polar results of the experiment.

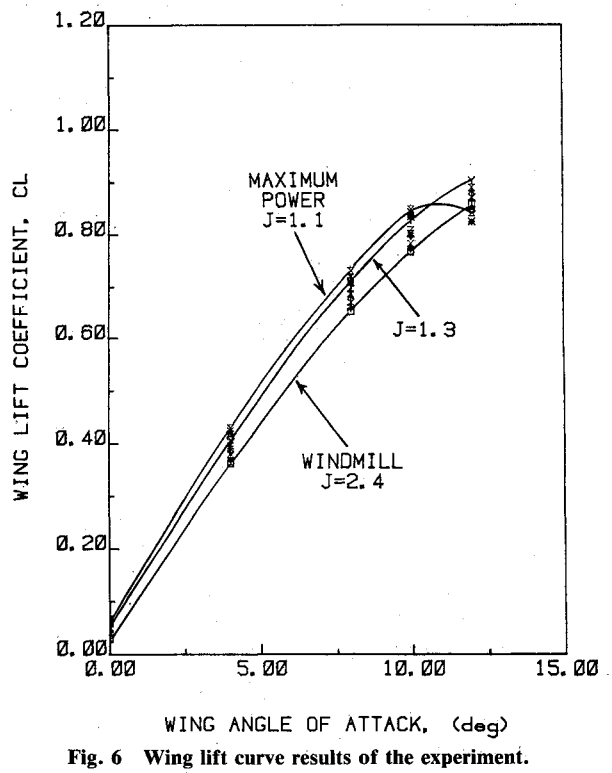

Fig. 6 Wing lift curve results of the experiment.

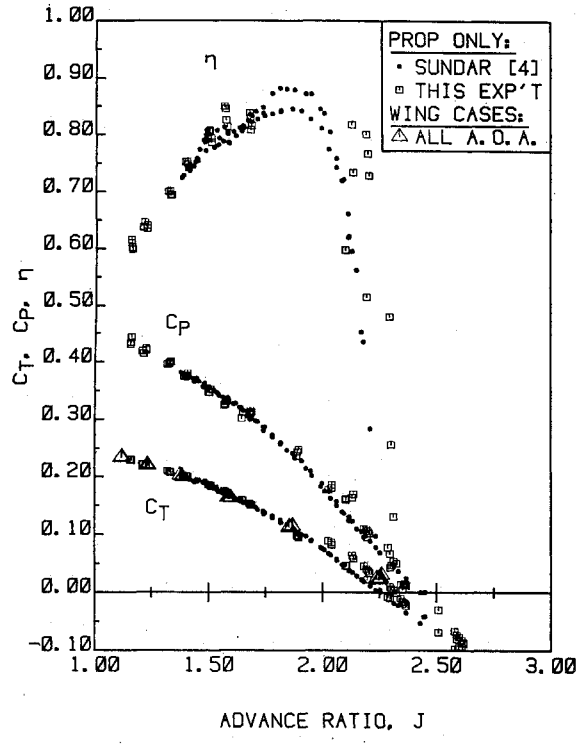

Fig. 7 Experimental propeller results.

by struts, the wing drag had to be corrected for the strut interference drag.

The propeller used in this experiment was a two-bladed Purdue model with a constant chord of 2 in., a diameter of 12 in., and an aspect ratio of 6. The propeller had a Goldstein's minimum induced-loss twist distribution. The propeller hub and nacelle diameters were 2 in. The blade airfoil section was a NACA 0010, and the pitch angle at the 3/4 radius location was set a 45.4 deg. The shaft was driven by a timing belt linked to a three-phase ac electric motor mounted under the tunnel floor. The thrust and torque of the propeller were measured by a two-component electric stain-gauge balance. The thrust data obtained from the balance was corrected for spinner drag. The propeller rotational speed was measured using an optical encoder. A combined wind screen and nacelle structure was fitted over the propeller drive system in order to shield this system from the airflow and reduce the strut interference on the propeller and wing.

Test Conditions

All tests were conducted under approximately incompressible conditions at a dynamic pressure of 0.1 psi. This provided a freestream velocity of approximately 115 ft/s and $M = 0.1$. The test Reynolds number was 470,000 based on a wing chord of 8 in. Propeller speeds were varied from windmill (48 rps, $J = 2.4$) to 100 rps at maximum power ($J = 1.1$). Wing angle of attack was varied from 0 to +13 deg.

Experimental Results

Wing Performance

The effect of interaction on wing performance can be seen in the drag polar plots of Fig. 5, which shows several individual polars for different propeller advance ratios. This figure clearly illustrates the anticipated trends of augmented lift and diminished drag for increasing propeller power (decreasing J) as a shift of the curves to the right and down. The data indicates that wing drag coefficient for this configuration can be reduced up to 155 counts at $C_L = 0.8$ and maximum propeller power ($J = 1.1$). Drag was reduced by a maximum percentage of 81% at $C_L = 0$ and $J = 1.1$. At the more typical operating C_L of 0.4, drag was reduced up to 67%.

The lift augmentation can clearly be seen in Fig. 6, the plot of lift curves for various advance ratios. It appears that an "effective camber" is present as a result of interaction since the lift curves have a vertical offset at an angle of attack of 0 deg, $\Delta C_L = 0.0386$ for $J = 1.1$. In addition, if a linear fit is applied to the lift data for angles of attack below 8 deg, it can be seen that the lift curve slope is increased 5.6% at full power.

The previous comparisons were made between powered cases and the windmill or zero power condition rather than reference the isolated wing case. This was done since the windmill data and the isolated wing data were virtually identical to within the error of the experiment.

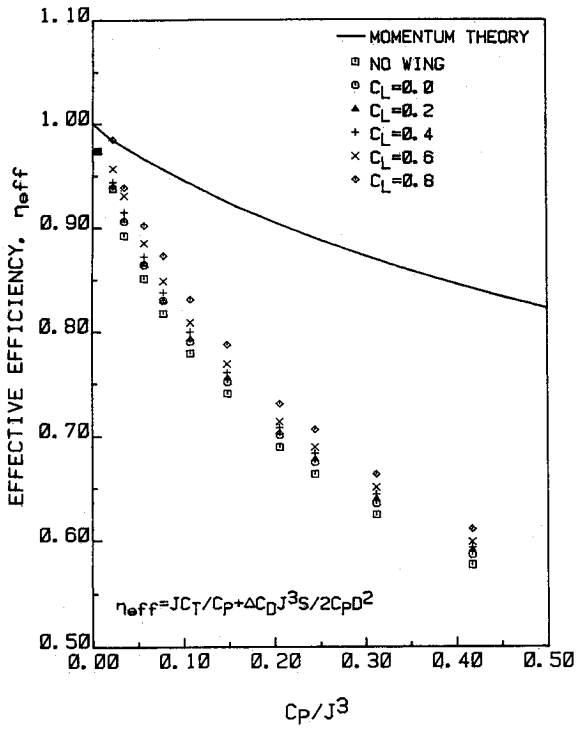

Fig. 8 Effective efficiency results from the experiment.

Propeller Performance

The interaction effects experienced by the propeller can be seen in the plot of Fig. 7. This figure shows how propeller thrust coefficient varies with the advance ratio as the wing angle of attack changes. This figure also shows isolated propeller data taken by Sundar[4] and by the present investigators for comparison. Unfortunately, power coefficient results were only available for the isolated propeller since the torque balance exhibited a significant sensitivity to the interaction-induced side force on the propeller.

The results indicate that the interactive effect on propeller thrust is indeed very small. If the thrust is modified at all it seems to be smaller than the scatter of the data, which is on the order of 3% for low advance ratios. However, at the high advance ratios the scatter is of the same order of magnitude as the thrust. Thus, any modification of the thrust loading at these high advance ratios cannot be determined conclusively.

Although the power results for the interactive case could not be measured directly, it was determined that the power input does not change significantly near the windmill point as wing loading is varied. This conclusion was made after measuring the propeller rotational speed at the windmill point as wing angle of attack was changed. The results indicated that the windmill advance ratio remained constant.

Combined Performance for the Tractor Configuration

It should be noted from the previous data that the power input to the propeller must be large to gain the large drag reductions on the wing. However, at such conditions of high power, propulsive efficiency drops off rapidly (Fig. 7). Therefore, a more representative measure of the performance benefit obtained from the combined configuration would include performance information from both the propeller and the wing. The performance parameter chosen for this investigation is the effective propulsive efficiency,

$$\eta_{\text{eff}} = JC_T/C_P + \Delta C_D J^3 S/2C_P D^2 \qquad (1)$$

Essentially, η_{eff} is simply the propeller propulsive efficiency if the wing drag reduction is treated as a propeller thrust augmentation. The effective efficiency was calculated assuming that propeller performance was not altered. This allowed the use of the isolated propeller data in the calculation of this parameter. A plot of η_{eff} vs a propeller power factor is shown in Fig. 8. From this data, it can be seen that the effective efficiency improvement is maximized for the lower power inputs. The maximum $\Delta\eta_{\text{eff}}$ is 5.5% for $C_P/J^3 = 0.0788$ ($J = 1.6$) and $C_L = 0.8$. However, even if the propeller is highly loaded, the effective efficiency improvement is as high as 3–4%.

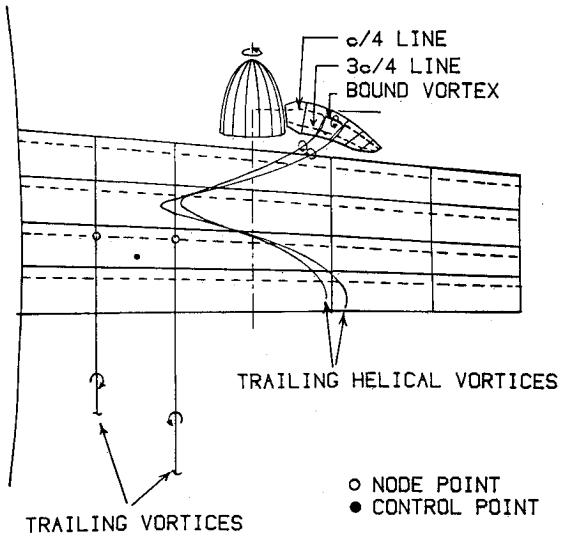

Fig. 9 Sketch of the vortex geometry for vortex lattice modeling of propeller-wing interaction.

Computational Analysis

A computational analysis of propeller-wing interaction was performed using two separate methods. The first method was the semiempirical design code that was previously described in the Design Philosophy section. The second method was a vortex lattice simulation of both the propeller and the wing as described in the following.

Description of Vortex Lattice Simulation of Propeller and Wing

A vortex lattice method (VLM) capable of calculating steady and quasisteady performance of a propeller and wing combination was developed. In this method, both the propeller and the wing are discretized into panels, which are modeled by a bound vortex segment at the quarter chord and wake vortices that trail from the bound segment endpoints. The propeller wake is assumed to be a rigid helix of constant diameter and the wing wake is assumed to be flat and to lie in a plane parallel to the streamwise direction. The flow tangency boundary condition is applied at the control points, which are located on the midpoint of the 3/4 chord line of each panel on both the propeller and wing. The model arrangement as described is shown in Fig. 9. Details concerning geometry specification and application of the VLM to propellers have been addressed by several authors.[7–12] Discussion of the method as applied to the mutually interactive counter-rotating system has been done by Lesieutre.[13] Application of the vortex lattice model to the propeller and wing combination is very similar to the counter-rotation problem except for nonaxisymmetry considerations. Since the wing geometry is nonaxisymmetric with respect to the propeller axis of rotation, wing interference will act to create different loadings on the separate blades of a propeller.

After the induced-velocity expressions are calculated and the flow tangency boundary conditions are applied, a system of equations is generated in the following form for a two-bladed single rotating propeller and wing:

$$\begin{bmatrix} [A_{11}] & [A_{21}] & [A_{w1}] \\ [A_{12}] & [A_{22}] & [A_{w2}] \\ [A_{1w}] & [A_{2w}] & [A_{ww}] \end{bmatrix} \begin{Bmatrix} \{\Gamma_i^1\} \\ \{\Gamma_i^2\} \\ \{\Gamma_i^w\} \end{Bmatrix} = \begin{Bmatrix} \{b_i^1\} \\ \{b_i^2\} \\ \{b_i^w\} \end{Bmatrix} \qquad (2)$$

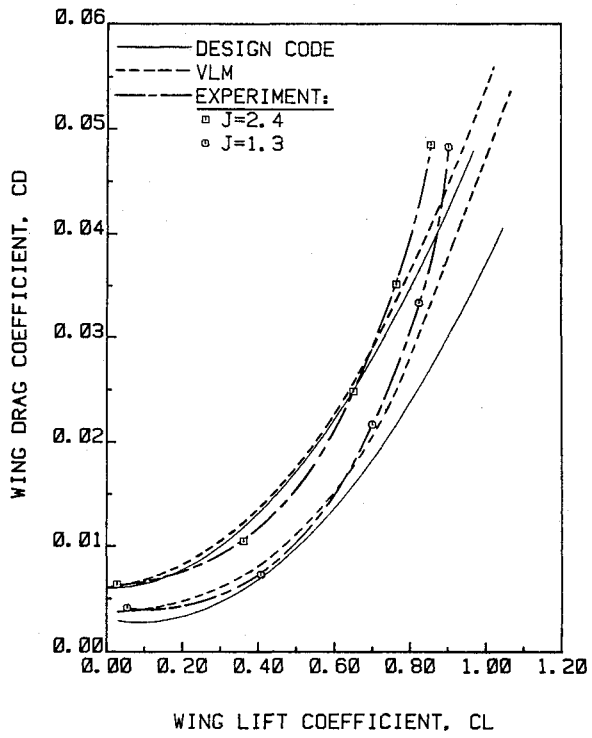

Fig. 10 Comparison of the experimental and analytical drag polars.

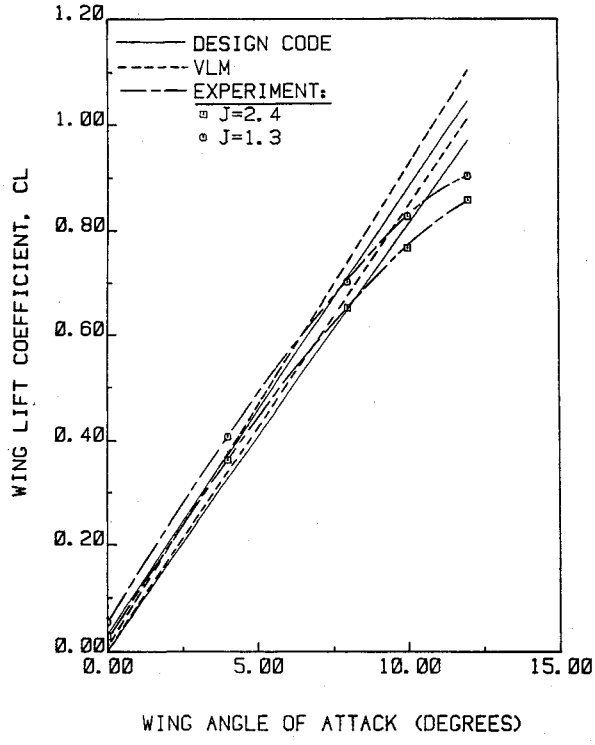

Fig. 11 Comparison of the experimental and analytical lift curves.

The matrices A_{11}, A_{22}, and A_{ww} are the self-induced influences of the first blade, second blade, and the wing on itself, respectively. The off-diagonal terms are mutual interference terms (i.e., A_{2w} is the influence matrix of the second blade on the wing). The above system must be solved separately for different phase angles between propeller blade 1 and the wing.

Forces on each bound vortex element are calculated using the Kutta-Joukowski law for each phase angle. The result is the quasisteady loading on both the propeller and wing. The steady results are obtained simply by averaging the quasisteady results over one propeller revolution. In order to compare

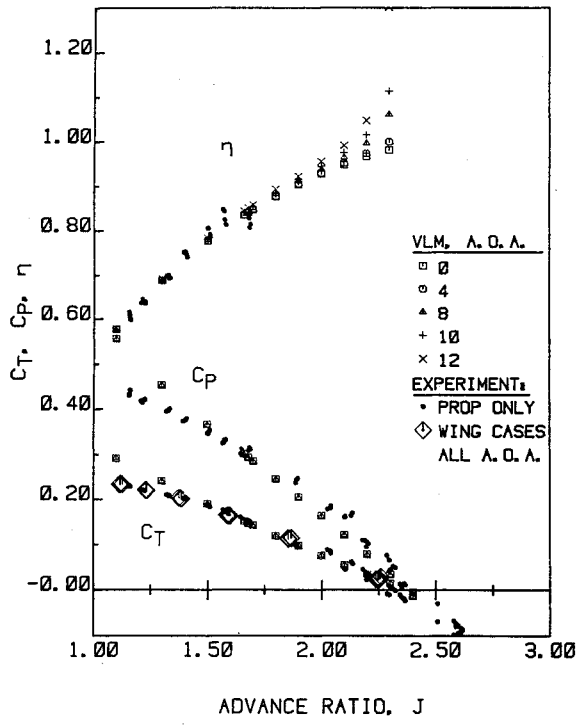

Fig. 12 Comparison of computational and experimental propeller results.

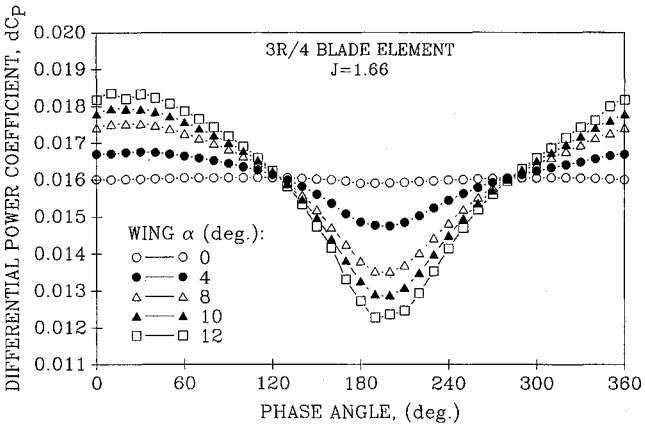

Fig. 13 Quasisteady, differential propeller power loading results from the vortex lattice method (¾R element).

results to the experiment wing, viscous drag was added in a manner similar to the semiempirical model.

Comparison and Discussion of Computations and Experiment

Both computational codes were run using the geometry of the experimental test setup. The propeller and wing performance results of the analysis are compared to the data and evaluated in this section. In addition, the quasisteady results of the vortex lattice method are presented and discussed here.

Wing Performance

The drag polars for the cases of windmill ($J=2.4$) and $J=1.3$ are shown in Fig. 10 for both of the codes and the experiment. From the figure, it can be seen that the agreement with the test is good for both computational methods at lower wing angles of attack ($C_L<0.65$). The semiempirical model tends to overpredict the drag reduction by 10–30%. However, the VLM's drag prediction seems to differ from the test by only 6–12% at these low angles of attack. At higher angles, the analytical results start to deviate from the experiment since the

local angles in the upwash region of the propeller wake are large enough to generate nonlinear behavior in those areas.

The comparison of lift curves can be seen in Fig. 11, for $J = 2.4$ and 1.3. Here it can be seen that the lift augmentation is overpredicted slightly by both codes. For example, the semiempirical method predicts a lift increase of 14% at 8 deg, whereas the vortex lattice model predicts an 11% increase. However, the experiment indicates a lift increase of only 8% at the same angle of attack.

Propeller Performance

The comparison of thrust and power coefficients and efficiency vs advance ratio is shown in Fig. 12. The semiempirical results do not apply here since propeller performance was assumed to be unaffected by the wing interference. The VLM appears to do a good job of predicting propeller performance above an advance ratio of $J = 1.4$. However, at higher power settings, the code overpredicts the thrust and the power consumed, but the efficiency shows good agreement at these low advance ratios. The results of the code indicate that propeller performance improvement increases as power is decreased. It should be noted that viscous effects were not included in the propeller performance calculations. Thus, the efficiency does not drop off near $J = 2.00$ as the measurements of Fig. 7 indicate. Therefore, it must be assumed that the advance ratio of maximum performance is near 2.00 and the predicted performance at higher J is unrealistic. At $J = 2.00$, the maximum computed thrust augmentation is 1.5%, the maximum power reduction is 0.7%, and the efficiency is increased by approximately 2%. It should be noted that both the experiment and the VLM indicate that the change in steady propeller loading is very small for this configuration. Additionally, since the propeller location is closer to the wing than in typical configurations, it can be estimated that the interference effect on steady propeller performance is negligible. Thus, the assumption of the semiempirical model was reasonable.

Quasisteady Results of VLM

The quasisteady propeller blade differential power loading at the 3/4 radius element of blade 1 as predicted by the VLM is shown in Fig. 13. The quasisteady propeller-blade differential thrust loading results are very similar to the power loading results. The phase angle is defined as the angle between the blade 1 bound vortex and the wing bound vortex and is 0 when the blade is in the plane of the wing on the outboard side. The blade loadings clearly indicate an asymmetric loading on the blades of the propeller as a result of the interaction. This is to be expected since the propeller is operating in an upwash field induced by the wing. As previously discussed in the Design Philosophy section, the upwash acts to augment loading on the outboard blade and to degenerate the loading on the inboard blade. This asymmetric loading can result in forced propeller vibration and noise generation.

Conclusion

A complementary experimental and computational investigation of propeller/wing interaction has been conducted to determine the steady performance change of a tractor configuration. The propeller used in this investigation was a two-blade Purdue model, and the wing was an unswept, untapered semispan model.

The experimental tests indicated that the wing performance can be improved significantly. The benefits include drag reduction and lift augmentation. Some typical wing results include a drag reduction of 65% at $C_L = 0.4$ and a C_{L_α} increase of 5.6%. Additionally, the interference effect on propeller performance was observed to be small especially at low advance ratios. When the propeller and wing results were combined in an effective efficiency, it was discovered that the maximum benefit of interaction occurs at the lower power conditions. It was also revealed that the effective propulsive efficiency of this configuration could be increased up to 3–5% from interactive effects.

The computational analysis showed that the performance trends can be calculated effectively with two separate methods. Reasonably accurate results (10–30% for ΔC_D) for the wing were obtained with a simple, fast, semiempirical code. However, more accurate agreement was obtained from the vortex lattice method (6–12% for ΔC_D) for both the wing and the propeller. Additionally, quasisteady results indicating an asymmetric loading on the propeller could be obtained from the VLM.

Acknowledgment

The authors would like to acknowledge the support of NASA Lewis Research Center under Grant NSG-3134.

References

[1]Kroo, I., "Propeller-Wing Integration for Minimum Induced Loss" AIAA Paper 84-2470, Oct. 1984.

[2]Miranda, L. R. and Brennan, J. E., "Aerodynamic Effects of Wingtip-Mounted Propellers and Turbines," AIAA Paper 86-1802, July 1986.

[3]Patterson, J. C. and Bartlett, G. R., "Effect of a Wingtip-Mounted Pusher Turboprop on the Aerodynamic Characteristics of a Semispan Wing," AIAA Paper 85-1286, July 1986.

[4]Sundar, R. M., "An Experimental Investigation of Propeller Wakes Using a Laser Doppler Velocimeter," Ph.D. Thesis, Purdue Univ., West Lafayette, IN, Dec. 1980.

[5]Witkowski, D. P., "An Experimental Investigation of the Aerodynamic Interaction Between Propellers and Wings," Master's Thesis, Purdue Univ, West Lafayette, IN, Aug. 1988.

[6]Abbott, I. H. and von Doenhoff, A. E., *Theory of Wing Sections,* Dover, New York, 1949, pp. 462–463.

[7]Baskin, V. B., Vil'dgrube, L. S., Vozhdayeu, Ye. S., and Maykapar, G. I., "Theory of the Lifting Airscrew," NASA Technical Translation F-823, Feb. 1976.

[8]Bober, L. J. and Chang, L. K., "Factors Influencing the Predicted Performance of Advanced Propeller Designs," NASA TM-82676, July 1981.

[9]Chang, L. K., "The Technical Performance of High Efficiency Propellers," Ph.D. Thesis, Purdue Univ., West Lafayette, IN, Dec. 1980.

[10]Chang, L. K. and Sullivan, J. P., "Optimization of Propeller Blade by an Analytical Method," AIAA Paper 82-1125, Feb. 1982.

[11]Egolf, T. A., Anderson, O. L., Edwards, D. E., and Landgrebe, A. J., *An Analysis for High-Speed Propeller-Nacelle Aerodynamic Performance Prediction: Vol. 1, Theory and Initial Application and Vol. 2, User's Manual for the Computer Program*, United Technologies Research Center, East Hartford, CT, r79-912949-19, June 1979.

[12]Sullivan, J. P., "The Effect of Blade Sweep on Propeller Performance," AIAA Paper 77-0716, June 1977.

[13]Lesieutre, D. J., "The Theoretical Performance of Counter-rotating Propeller Systems," Master's Thesis, Purdue Univ., West Lafayette, IN, May 1985.